Super-Resolution SERS Spectral Bioimaging

Zachary D. Schultz*[a], Deben N. Shoup[a], Abigail E. Smith[a]
[a] Department of Chemistry and Biochemistry, The Ohio State University, 100 W. 18th Avenue, Columbus, OH, USA 43210-1173

ABSTRACT

Advances in nanotechnology enable the detection of trace molecules from the enhanced Raman signal generated at the surface of plasmonic nanoparticles. We have developed technology to enable super-resolution imaging of plasmonic nanoparticles, where the fluctuations in the surface enhanced Raman scattering (SERS) signal can be analyzed with localization microscopy techniques to provide nanometer spatial resolution of the emitting molecule's location. Additional work now enables the super-resolved SERS image and the corresponding spectrum to be acquired simultaneously. Here we will discuss how this approach can be applied to provide new insights into biological cells.

Keywords: SERS, plasmonics, biological, microscopy, super-resolution, Raman, imaging

1. INTRODUCTION

Interest in optically detecting and imaging molecules has led to pioneering advances in chemical microscopy.[1] Molecules that fluoresce are routinely detected at the single molecule level and new advances in imaging instrumentation and data processing now enable imaging with spatial resolution well below the classical diffraction limit. One such approach is stochastic optical reconstruction microscopy (STORM),[2] which uses temporal fluctuations from single emitters to mark the centroid of emission from nanometer scale objects in order to generate a high spatial resolution image from the data. The development of optical probes that can be turned on, or activated, and then turned off, or deactivated, has enabled STORM imaging of numerous structures, and increased the use of localization algorthms in biological imaging.

To image molecules that do not fluoresce, other approaches are needed. Vibrational spectroscopy leverages the unique combination of chemical bonds in a molecule to provide highly specific chemical detection. The energy levels typically associated with vibrational modes are associated with photons that have wavelengths on the order of several micrometers. Raman scattering arises from the inelastic scattering of light from molecules, where the energy difference between the incident and scattered light correlates with the vibrational modes of the sample. Raman can be elicited using visible lasers; however, the cross-section of most Raman processes is very low and sensitive detection is challenging.

Plasmonic nanostructures have been shown to amplify the Raman signal from molecules in close proximity to the surface of a nanostructure, an effect that is commonly referred to as surface enhanced Raman scattering (SERS).[3, 4] When the nanostructure is confined to the tip of a scanning probe microscope (SPM), so called tip-enhanced Raman scattering (TERS), nanoscale imaging can be obtained.[5] The concentration of the electric field and reradiation of the scattering from molecules near the surface of the structure transform Raman into an ultrasensitive detection method.[6] Single molecules have been detected by SERS,[7, 8] and in the last decade TERS imaging has been demonstrated with sub-nanometer resolution providing intramolecular information from molecules in ideal conditions.[9, 10] For bioimaging, the necessary interaction between the SPM tip and biological samples complicates analysis; however, molecules on the surface of cells have been imaged and detected with TERS.[11-13]

An interesting alternative is to combine localization microscopy with the Raman signals observed from plasmonic nanostructures.[14] It has been shown that the position of a single Raman scattering molecule on the surface of a nanoparticle can be tracked with using localization microscopy similar to STORM.[15] Plasmonic nanoparticles undergo intensity fluctuations,[16] which simplifies STORM analysis using the intrinsic signal fluctuations to isolate the position of individual molecules. Indeed, electromagnetic hotspots, or areas of intense Raman scattering, on the surface of nanoparticles have been spatially resolved using super-resolution SERS imaging.[17] It was further demonstrated that

*schultz.133@osu.edu; phone 1 614 292-5775; https://research.cbc.osu.edu/schultz.133/

protein receptors binding to peptide-functionalized gold nanoparticles could be imaged in biological cells, providing nanoscale spatial resolution in a wide-field format.[18]

In super-resolution SERS imaging, the Raman scattered photons are binned to provide sufficient intensity to be detected and monitored, but binning the signal sacrifices the chemical information present in the spectrum. For sufficiently bright optical signals, it is possible to collect the image and the spectrum simultaneously by placing a diffraction grating in close proximity to the array detector used for image acquisition. This approach has been called snapshot or spectral imaging and has been used to correlate spectra with images in fluorescence, electronic scattering, and SERS imaging.[19-23] Our group has adapted this approach to monitor the SERS signals emitted from individual plasmon nanoparticles, providing a method to validate the detection of nanoparticles and suggesting a route to monitor chemical interactions within living cells. The report will present how this super-resolution SERS spectral imaging approach works and can be applied in bioimaging experiments.

2. METHODOLOGY

2.1 Raman Microscope.

The Raman microscope has been described previously but is summarized here for clarity.[24] The instrument is built around an Olympus IX-71 inverted microscope frame. The sample sits in the horizontal plane and the objective from the inverted microscope is used to collect the optical signal from the samples. The laser excitation is provided by a 300 mW 659 nm single longitudinal mode diode laser (Laser Quantum). The laser is directed from above the sample, providing a transmission style set-up, and is focused to an approximately 30 μm diameter spot using a f=75 mm singlet lens. The image collected from the wide-field illumination is passed through a 638 nm longpass dichroic mirror (Thorlabs) and a 660 longpass edge filter (Semrock). The image is focused by the tube lens through a 300 gr/mm transmission grating blazed at 17.5° (Thorlabs) and onto a scientific complementary metal-oxide semiconductor array (sCMOS, Hamamatsu Ltd., ORCA-Flash 4.0 V2)

2.2 Calibration.

Figure 1 illustrates the instrument set up. The transmission grating located immediately prior to the sCMOS detector diffracts the image into corresponding diffraction orders. The position of the sCMOS sensor is slightly offset with respect to the imaging path, such that the un-diffracted (n=0) image is captured on the first third of the imaging sensor. The n=1 diffraction signal is then captured on the remainder of the sensor. The distance between the transmission grating and sensor is determined using the geometric relationships between the n=0 and n=1 diffraction peaks of the 659 nm laser. We determine the angle r between the n=0 and n=1 diffraction peaks as follows:

$$\mathrm{n}\,\lambda = d\,(\sin r + \sin i) \tag{1}$$

Where n is the diffraction order, λ is the wavelength, d is groove spacing (nm/gr) of the grating, r is the angle of transmitted light, and i is the incident angle of the laser to the grating. At normal incidence, i= 0 degrees, and sin i = 0. From this you can calculate the angle at which n=1 diffraction is observed:

$$r = \sin^{-1}\left(\frac{\mathrm{n}\,\lambda}{d}\right) \tag{2}$$

By determining the angle of the n=1 diffraction, you can calibrate the exact distance from the sensor to the grating (l) by counting the number of pixels between the diffraction spots and multiplying by the pixel size as follows:

$$\mathrm{l} = \frac{(\#pixels\ *pixel\ size)}{\tan r} \tag{3}$$

The distance from the sensor to the grating is equivalent to the focal length in the equation commonly used to calculate reciprocal linear dispersion (D^{-1}):

$$D^{-1} = \frac{d}{\mathrm{n}\,l} \tag{4}$$

Note that here the assumption is made that cos r term is negligible. Once you have D^{-1}, one can covert the pixel spacing the sensor to wavelength.

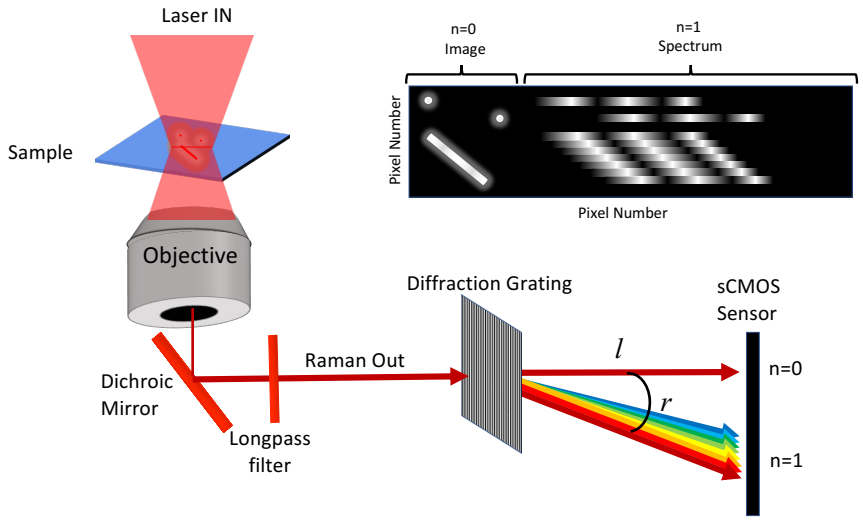

Figure 1. The figure illustrates the experimental set-up used for the wide-field spectral SERS imaging. The excitation laser is focused to a large spot at the sample, which is imaged by the microscope. The Raman scattering is filtered from the transmitted and Rayleigh scattered light and then dispersed by a transmission diffraction grating onto a sCMOS array sensor. The distance between the grating and the sensor (l), and the angle (r) of n=1 diffraction are important parameters for calibrating the spectral response. A cartoon illustration of the expected data is shown.

3. RESULTS

Figure 2A shows the results from illuminating a 5 μm pinhole with a neon calibration lamp. The location of the pinhole was moved to two different locations in the illuminated spot as shown in the composite image. The n=0 portion of the image is seen as a spherical signal. The spacing (l) between the grating and the sensor determines how much of the sensor will be used for imaging. The illumination spot can be adjusted to occupy a larger or smaller area. The n=1 portion of the spectrum corresponds to the wavelength dispersed light incident on the sensor array. Using the calibration method described above the distance between the grating and sensor was determined, l = 31 mm, and with a pixel size of 6.5 μm, the pixels from the n=0 signals were converted to wavelengths as shown in **Figure 2B**.

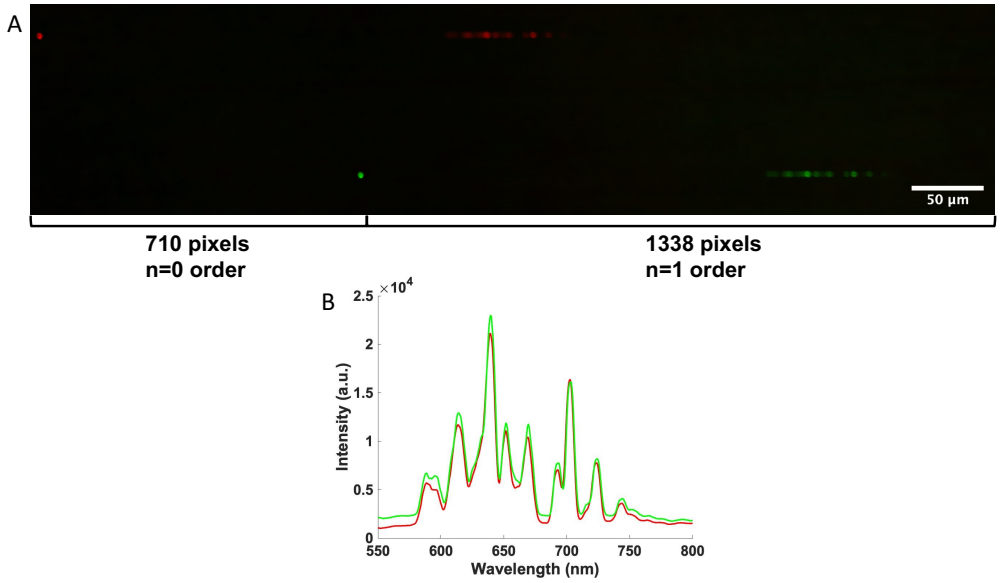

Figure 2. A) Composite image of a 5 μm pinhole imaged with a 20x objective located at two different points in the field of view. The pinhole was illuminated with a neon calibration lamp and the spectrum is recorded in the n=1 portion of the signal. **B)** The two spectra observed in A are plotted on the same axis applying the calibration to covert the peaks to wavelength.

In addition to providing an example of the collected data, Figure 2 illustrates two key points about the measurement. The n=1 diffraction spatially correlates with the location of the n=0 object. This has been shown to impact the spectral resolution, as the object acts as a virtual slit and the width of the n=1 features are the combination of the object with and D^{-1}.[24] **Figure 2** also illustrates a second important aspect of this imaging approach. If the objects are on the same row of pixels and closely spaced, the spectra in the n=1 portion of the sensor will overlap and complicate spectral analysis. The typical Raman spectrum of 100 – 3300 cm^{-1} typically correlates with about 100 nm of bandwidth, suggesting that the objects on the same row of pixels need to be more than 150 pixels apart, which corresponds to ~100 μm apart physically for the 6.5 μm pixels on our sensor. It is also worth noting in Figure 2B that the spectra obtained from different portions of the field of view show the same response.

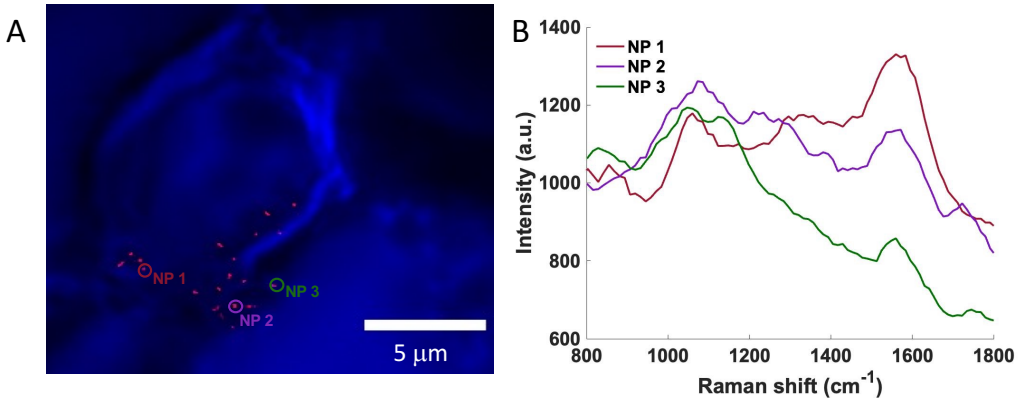

Figure 3. A) The brightfield image of a cell incubated with gold nanoparticles functionalized with a mercaptobenzoic reporter molecule and silica encapsulation is overlaid with the STORM fitting result. The nanoparticles are observed with increased spatial resolution. **B)** The spectral response from the 3 nanoparticles noted in (A) are plotted. The prominent Raman bands at 1080 cm^{-1} and 1600 cm^{-1} associated with the reporter molecule are clearly visible.

Because the spectral resolution corresponds to the object size on the sCMOS sensor, nanoparticle probes and their SERS response can be detected with decent spectral resolution. **Figure 3** results from a cell incubated with mercaptobenzoic acid functionalized gold nanoparticles. The power at the sample was 33 mW and the image was acquired by collecting 1000 frames at 10Hz. The SERS intensity fluctuations enable STORM algorithms to be applied. The ThunderSTORM plugin available in image J was used to localize the emission from the nanoparticles used here.[25]

To distinguish between nanoparticles and other emissive particles in the cell, the spectral response can be analyzed. Here the prominent ring stretches associated with the mercaptobenzoic acid reporter molecule can be clearly distinguished. NP2, which lies in a more congested portion of the image, shows evidence of other interfering signals; however, detection of the most intense Raman bands at the appropriate frequencies can distinguish this nanoparticle from others.

The ability to detect the Raman signal from particles in cells suggests new opportunities to probe the chemical interactions associated with proteins and other molecules found in cells. The nanoparticles can be located with high spatial resolution, and unlike TERS, the signals from within cells and tissues can be observed readily.

4. CONCLUSIONS

We have presented results illustrating how wide-field spectral, or snapshot, imaging can be used with SERS to provide high spatial resolution and chemical information from nanoparticle probes in biological systems. Calibration of the optical response provides Raman signals that can be used to differentiate nanoparticles from the cellular environment. Optimization of the enhancement associated with different nanoparticle probes suggests new methods to probe chemistry in biological samples.

5. ACKNOWLEDGMENT

This work was supported by the National Science Foundation award CHE-2107791 and the National Institute of General Medical Sciences award R01 GM109988.

REFERENCES

[1] L. Xiao, and Z. D. Schultz, "Spectroscopic Imaging at the Nanoscale: Technologies and Recent Applications," Anal Chem, 90(1), 440-458 (2018).

[2] M. J. Rust, M. Bates, and X. Zhuang, "Sub-diffraction-limit imaging by stochastic optical reconstruction microscopy (STORM)," Nature Methods, 3(10), 793-796 (2006).

[3] J. Langer, D. Jimenez de Aberasturi, J. Aizpurua *et al.*, "Present and Future of Surface Enhanced Raman Scattering," ACS Nano, 14(1), 28-117 (2019).

[4] D. L. Jeanmaire, and R. P. Van Duyne, "Surface raman spectroelectrochemistry: Part I. Heterocyclic, aromatic, and aliphatic amines adsorbed on the anodized silver electrode," Journal of Electroanalytical Chemistry and Interfacial Electrochemistry, 84(1), 1-20 (1977).

[5] R. M. Stockle, Y. D. Suh, V. Deckert *et al.*, "Nanoscale chemical analysis by tip-enhanced Raman spectroscopy," Chemical Physics Letters, 318(1-3), 131-136 (2000).

[6] Z. D. Schultz, J. M. Marr, and H. Wang, "Tip enhanced Raman scattering: plasmonic enhancements for nanoscale chemical analysis," Nanophotonics, 3(1-2), 91-104 (2014).

[7] K. Kneipp, Y. Wang, H. Kneipp *et al.*, "Single Molecule Detection Using Surface-Enhanced Raman Scattering (SERS)," Physical Review Letters, 78(9), 1667-1670 (1997).

[8] S. M. Nie, and S. R. Emery, "Probing single molecules and single nanoparticles by surface-enhanced Raman scattering," Science, 275(5303), 1102-1106 (1997).

[9] R. Zhang, Y. Zhang, Z. C. Dong *et al.*, "Chemical mapping of a single molecule by plasmon-enhanced Raman scattering," Nature, 498(7452), 82-86 (2013).

[10] L. Li, J. F. Schultz, S. Mahapatra *et al.*, "Chemically identifying single adatoms with single-bond sensitivity during oxidation reactions of borophene," Nature Communications, 13(1), 1796 (2022).

[11] L. Xiao, K. A. Bailey, H. Wang *et al.*, "Probing Membrane Receptor–Ligand Specificity with Surface- and Tip-Enhanced Raman Scattering," Analytical Chemistry, 89(17), 9091-9099 (2017).

[12] L. Xiao, H. Wang, and Z. D. Schultz, "Selective Detection of RGD-Integrin Binding in Cancer Cells Using Tip Enhanced Raman Scattering Microscopy," Analytical Chemistry, 88(12), 6547-6553 (2016).

[13] H. Wang, and Z. D. Schultz, "TERS detection of alphaVbeta3 integrins in intact cell membranes," Chemphyschem, 15(18), 3944-9 (2014).

[14] K. A. Willets, A. J. Wilson, V. Sundaresan *et al.*, "Super-Resolution Imaging and Plasmonics," Chemical Reviews, 117(11), 7538-7582 (2017).

[15] S. M. Stranahan, and K. A. Willets, "Super-resolution Optical Imaging of Single-Molecule SERS Hot Spots," Nano Letters, 10(9), 3777-3784 (2010).

[16] D. P. dos Santos, M. L. A. Temperini, and A. G. Brolo, "Intensity Fluctuations in Single-Molecule Surface-Enhanced Raman Scattering," Accounts of Chemical Research, 52(2), 456-464 (2019).

[17] N. C. Lindquist, C. D. L. de Albuquerque, R. G. Sobral-Filho *et al.*, "High-speed imaging of surface-enhanced Raman scattering fluctuations from individual nanoparticles," Nat Nanotechnol, 14(10), 981-987 (2019).

[18] C. D. L. de Albuquerque, and Z. D. Schultz, "Super-resolution Surface-Enhanced Raman Scattering Imaging of Single Particles in Cells," Analytical Chemistry, 92(13), 9389-9398 (2020).

[19] E. C. Heider, M. Barhoum, E. M. Peterson *et al.*, "Identification of Single Fluorescent Labels Using Spectroscopic Microscopy," Applied Spectroscopy, 64(1), 37-45 (2010).

[20] A. Al-Zubeidi, B. S. Hoener, S. S. E. Collins *et al.*, "Hot Holes Assist Plasmonic Nanoelectrode Dissolution," Nano Letters, 19(2), 1301-1306 (2019).

[21] M. N. Bongiovanni, J. Godet, M. H. Horrocks *et al.*, "Multi-dimensional super-resolution imaging enables surface hydrophobicity mapping," Nature Communications, 7(1), 13544 (2016).

[22] A. P. Olson, K. B. Spies, A. C. Browning *et al.*, "Chemically imaging bacteria with super-resolution SERS on ultra-thin silver substrates," Scientific Reports, 7(1), 9135 (2017).

[23] C. D. L. de Albuquerque, C. M. Zoltowski, B. T. Scarpitti *et al.*, “Spectrally Resolved Surface-Enhanced Raman Scattering Imaging Reveals Plasmon-Mediated Chemical Transformations,” ACS Nanosci Au*,* 1(1), 38-46 (2021).

[24] D. N. Shoup, B. T. Scarpitti, and Z. D. Schultz, “A Wide-Field Imaging Approach for Simultaneous Super-Resolution Surface-Enhanced Raman Scattering Bioimaging and Spectroscopy,” ACS Measurement Science Au, (2022). DOI: 10.1021/acsmeasuresciau.2c00013

[25] M. Ovesný, P. Křížek, J. Borkovec *et al.*, “ThunderSTORM: a comprehensive ImageJ plug-in for PALM and STORM data analysis and super-resolution imaging,” Bioinformatics*,* 30(16), 2389-2390 (2014).